Chapter 4

DETECTION OF THE PEROXY INTERMEDIATE IN THE OXIDATION OF 2-BUTENE BY THE NITRATE RADICAL (NO_3)

4.1 Introduction to NO_3 as a tropospheric oxidant

The free radical oxidation of volatile organic compounds (VOCs) drives the chemistry of the Earth's atmosphere. While most radicals are produced photochemically, the nitrate radical (NO_3) is formed by reaction:

$$NO_2 + O_3 \rightarrow NO_3 + O_2 \qquad (4.1)$$

During the daytime, NO_3 is destroyed by sunlight:[1]

$$NO_3 + h\upsilon \rightarrow NO + O_2 \qquad (4.2\ a)$$

$$+ h\upsilon \rightarrow NO_2 + O(^3P) \qquad (4.2\ b)$$

At nighttime, however, NO_3 is the main oxidant in the troposphere (~50 ppt), with various roles in gas phase chemistry reactions and secondary organic aerosol (SOA) formation.[2-20]

The oxidation of VOCs by NO_3 is directly related to the formation of peroxy radicals in the atmosphere. For alkanes (RH), hydrogen abstraction is the main reaction mechanism:

$$RH + NO_3 \rightarrow R + HNO_3 \qquad (4.3)$$

$$R + O_2 \rightarrow RO_2 \text{ (peroxy radical)} \qquad (4.4)$$

The peroxy radicals play key roles in pollutant and ozone formation. The different reaction pathways and the relationship of the radicals to other atmospheric networks have been discussed in Chapter 1. Significant research has been focused on characterizing the peroxy radicals and measuring their rates of reaction with atmospheric gas species.[3,21-26]

Less research has been devoted to the oxidation of alkenes by NO_3. Observations of products from NO_3-initiated oxidation of isoprene in SOAs however have sparked interest in the oxidation of alkenes.[6,7,9-12,14,18,19] Isoprene is the most abundant non-methane VOC in the atmosphere, with global emissions of ~500 Tg (C) yr^{-1}.[5] As isoprene is released mainly from deciduous trees during the day, its reaction with the NO_3 was long believed to be insignificant. The new studies however show that under cloudy conditions or near dusk, both NO_3 and isoprene levels are sufficiently high to be of atmospheric relevance.

NO_3 addition to the double bond of alkenes (R=R′) leads to competing pathways of epoxide and NO_3-substituted peroxy radical formation:

$$R{=}R' + NO_3 \rightarrow R\text{-}\ R'(NO_3) \qquad (4.5)$$

$$R\text{-}\ R'(NO_3) \rightarrow ROR' \text{ (epoxide)} + NO_2 \qquad (4.6\ a)$$

$$+ O_2 \rightarrow R\text{-}\ R'(NO_3)O_2 \text{ (nitrooxyalkyl peroxy radical)} \qquad (4.6\ b)$$

At low pressures, the epoxide channel (4.6 a) dominates, while at high pressures, the NO_3-peroxy radical channel (4.6 b) dominates.[13,27-41] NO_3-peroxy radicals undergo similar reaction pathways as the unsubstituted peroxy radicals; however, the reaction rates are not well-characterized. To date, only one theoretical paper has investigated the

potential energy surface (PES) of isoprene oxidation by NO_3 and the different branching ratios of NO_3-peroxy radical formation.[42] No experiment has ever detected for any alkene oxidation system the NO_3-peroxy radical intermediate in the gas phase.

While much attention has been given to the formation of peroxy radicals, the epoxide channel is also of atmospheric interest, especially with respect to SOA formation.[43-46] Epoxide rings can open in acidic mediums to produce volatile diol, sulfate ester, and polymer products. These products have all been observed in SOA field samples. The Intergovernmental Panel on Climate Change recently highlighted aerosols as one of the greatest uncertainties in the Earth's radiation budget.[47] The radiation budget plays a significant factor in global warming and climate modeling predictions. All atmospheric sources of epoxides must be taken into account.

The quantitative yields of the competing pathways of NO_3-initiated oxidation of alkene systems are highly debated. In the simple NO_3 + 2-butene system, estimates of the epoxide yields range from <1% to 20%.[4,27,29] The majority of these measurements were made in aerosol chambers, in which the final end products were analyzed hours after initiation of the reactions. Early intermediate and product detection could resolve some of the observed disparities. In particular, *in situ* detection of the NO_3-peroxy radicals would be useful.

In this work, we use the pulsed CRDS apparatus to detect the 2-NO_3-butyl peroxy radical in the oxidation of 2-butene by NO_3. We discuss in the next section why this reaction system was chosen and how we propose to detect the radical in the gas phase.

4.2 Detection of the 2-NO_3-butyl peroxy radical

4.2.1 The NO_3 + 2-butene system

The reaction rate constants of NO_3 with various alkenes have recently been reviewed.[4] While the NO_3-ethyl peroxy radical is the simplest and therefore prototype of the substituted NO_3 peroxy radicals, the measured rate constant for NO_3 addition to ethene is considerably slower than NO_3 addition to 2-butene and isoprene:

$k_{298\,K}$(ethene + NO_3) = 2.05 × 10^{-16} cm^3 $molec^{-1}$ s^{-1}
$k_{298\,K}$(*cis/trans*-2-butene + NO_3) = 3.52/3.90 × 10^{-13} cm^3 $molec^{-1}$ s^{-1}
$k_{298\,K}$(isoprene + NO_3) = 2.05 × 10^{-13} cm^3 $molec^{-1}$ s^{-1}. (4.7 a-c)

The potential energy surfaces (PES) of NO_3 addition to ethene and 2-butene have been investigated to explain the difference between the two rate constants.[48-52] The PES barrier for the NO_3-ethene adduct to dissociate back to the reactants is much lower than the barrier for the NO_3-2-butene adduct. None of the PES calculations however take into consideration the presence of oxygen. More theoretical work is needed on NO_3-initiated oxidation of alkenes under atmospheric conditions.

For this work, we chose NO_3 + 2-butene as the prototype alkene oxidation system. While other large alkenes have similar rates of reaction with NO_3, the inherent symmetry of 2-butene simplifies the detection problem to only one NO_3-peroxy radical. The chemical pathways of NO_3 + 2-butene and the associated peroxy radical reactions are shown in Fig. 4.1. For simplicity, reactions with other common peroxy radical species such as the hydroperoxy species (HO_2) have not

been included. Of the reactions shown, only the rate of NO_3 addition to 2-butene has been well-measured.

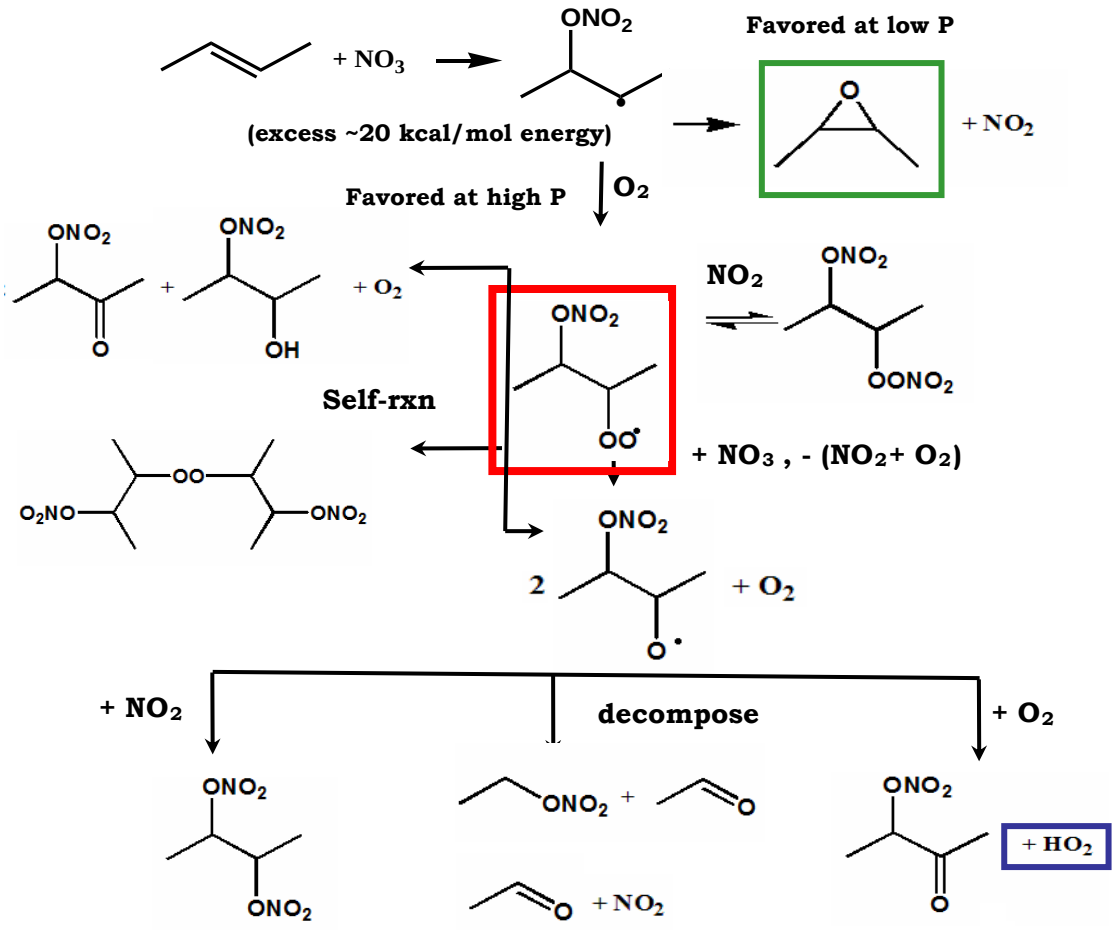

Figure 4.1. Schematics of the various chemical pathways of 2-butene oxidation by NO_3. The red and green boxes signify major products of the competing oxidation pathways, the 2-NO_3-butyl peroxy radical (red) and the epoxide product, oxirane (green). Although the reactive hydroperoxy radical HO_2 (blue box) is formed downstream, reactions with unsubstituted peroxy radicals have not been included in the reaction scheme for simplicity.

4.2.2 Detection of peroxy radicals

Peroxy radicals have generally been detected spectroscopically via the $\tilde{B} \leftarrow \tilde{X}$ transition in the ultraviolet (UV) region.[3,21-26] While absorption cross sections are quite large ($\sigma_{UV}(RO_2)$ = 10^{-16}~10^{-18} cm^2),[1] the spectral features tend to be broad and structure-less, as the PES for the upper $\tilde{B}$ state is a repulsive surface. Many peroxy radicals therefore have overlapping UV absorptions, complicating individual identification and quantification of the radicals (Fig. 4.2). In this work, we explore an alternate method to detect the peroxy radical.

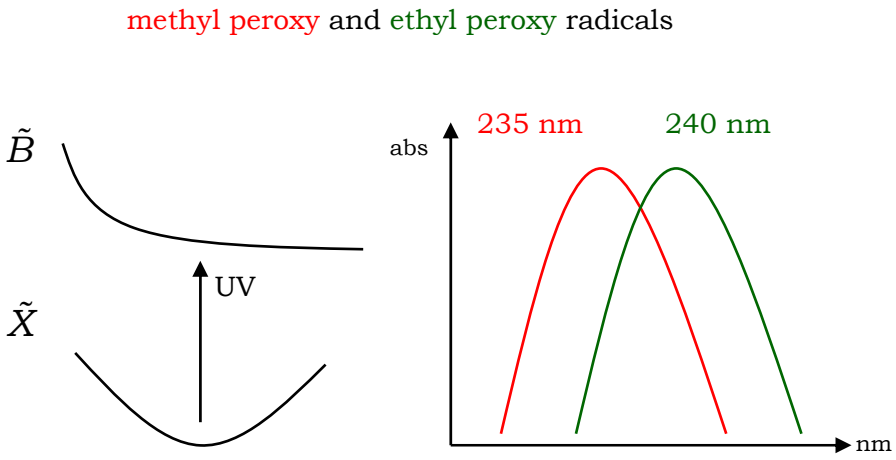

Figure 4.2. A cartoon representation of the UV transition from the bound ground $\tilde{X}$ state to the repulsive excited $\tilde{B}$ state surface (left). The resulting spectra for methyl and ethyl peroxy radicals are shown on the same plot (right). Overlap of the broad and non-distinctive absorptions complicates identification and quantification of the species.

Recent efforts have focused on detection of the peroxy radicals via the $\tilde{A} \leftarrow \tilde{X}$ transition in the near infrared (NIR) region.[53-61] Absorption cross sections are much weaker ($\sigma_{NIR}(RO_2)$ = 10^{-20}~10^{-21} cm^2); yet transitions to the bound $\tilde{A}$ state result in more structured spectral features. In a systematic study of alkyl peroxy radicals, the Miller group demonstrated that not only the isomers but also the different conformers of the same

structural peroxy radical isomer could be distinguished in the NIR spectra (7000-8000 cm^{-1}).[61] Each peroxy radical has a distinct $\tilde{A} \leftarrow \tilde{X}$ origin band and COO bend and COO stretch absorptions ~500 cm^{-1} and ~1000 cm^{-1} to the blue of the origin, respectively. The spectra of the smaller alkyl peroxy radicals showed narrow structured bands, while the spectra of the larger alkyl peroxy radicals contained broad absorptions (width ~500 cm^{-1}) with multiple bumps arising from overlap of the various conformers. *Ab initio* methods, including density functional theory (e.g., B3LYP) and Gaussian 2 Møller–Plesset 2 (G2MP2), were used with high quantitative accuracy to predict the origins of the $\tilde{A} \leftarrow \tilde{X}$ transitions of the alkyl peroxy radicals.

This spectroscopic approach has been extended to study the substituted peroxy radicals.[62-64] The origin of the $\tilde{A} \leftarrow \tilde{X}$ transition should shift to the red or blue of the parent peroxy radical depending on the electron-withdrawing or contributing nature of the substituent with respect to the OO moiety of the peroxy radical. The overall shape of the band should remain the same. In the extreme case of fluorinated methyl peroxy radical (CF_3O_2), the origin of the $\tilde{A} \leftarrow \tilde{X}$ transition shifted 727 cm^{-1} to the red of the origin of the methyl peroxy radical (CH_3O_2); the rotational contour of the band remained very similar.[63]

Our group has systematically studied the $\tilde{A} \leftarrow \tilde{X}$ transitions of Cl-alkyl peroxy radicals.[64] The origin bands were shifted slightly to the red of the origins of the respective unsubstituted alkyl peroxy radicals. B3LYP calculations were done in *Gaussian98* to predict the origins of the $\tilde{A} \leftarrow \tilde{X}$ transitions of the Cl-alkyl peroxy radicals.[65] Specifc details are provided in the thesis of a senior lab member.[64] Briefly, C-C-Cl and C-O-O dihedral angles were systematically varied, with geometry and energy

optimizations done at each scan point. At each minimum, the highest occupied alpha or beta orbital was manually adjusted in the Gaussian input file such that the overall symmetry of the radical was that of the excited state. The energy was then re-calculated and compared to the "ground state" energy value for determination of the origin band frequency. Theoretical results were consistent with experimental values, demonstrating that density functional theory could be applied to substituted peroxy radicals.

In the case of NO_3 addition to 2-butene, the number of electrons is too large for *ab initio* calculations. We instead use the previously published spectrum of the $\tilde{A} \leftarrow \tilde{X}$ transition of *sec*-butyl peroxy radical to predict the frequency of the origin band for the $\tilde{A} \leftarrow \tilde{X}$ transition of 2-NO_3-butyl peroxy radical.[54] The NIR spectrum of the *sec*-butyl peroxy radical shows a relatively broad absorption between 7350 cm^{-1} and 7750 cm^{-1}, with two distinct bumps at 7560 cm^{-1} and 7605 cm^{-1} for conformers A and B. Weak absorptions corresponding to the torsional motions are observed at 8051 cm^{-1} and 8507 cm^{-1}. We expect the origin band for 2-NO_3-butyl peroxy radical to be slightly red-shifted. We therefore conduct the pulsed CRDS experiments in the 7200-8600 cm^{-1} region.

4.3 Experimental conditions

4.3.1 The chemistry

Our goal is to detect the substituted NO_3-peroxy radical *in situ*. Typical NO_3 sources include discharge of fluorine in the presence of nitric acid (HNO_3), photolysis of chlorine nitrate ($ClONO_2$), and thermal decomposition of dinitrogen pentoxide (N_2O_5):

$$F + HNO_3 \rightarrow HF + NO_3 \quad (4.8)$$

$$ClONO_2 \rightarrow Cl + NO_3 \quad (4.9)$$

$$N_2O_5 + \Delta(heat) \rightarrow NO_2 + NO_3 \quad (4.10\ a)$$

In the first two methods, the F and Cl atom preferentially attack the alkene. Nitric acid concentrations cannot be increased significantly in to scavenge the F atoms in reaction 4.8, as nitric acid absorbs in the NIR region (Appendix 3.4). The third method is more plausible. The thermal decomposition of N_2O_5 was used as the NO_3 source for our study of the $\tilde{A}$ state of NO_3 (Chapter 3). Given our previous flow conditions, however, the residence time of the flow cell experiments is very long (~150 ms to 1 s). The lifetime of peroxy radicals is on the millisecond timescale such that secondary chemistry would complicate spectral detection (Appendix 4.1).

We therefore explored photolytic precursors of NO_3, as the NIR probe laser could be delayed on the microsecond timescale with respect to the excimer fire or chemical initiation. We searched for methods in which byproducts of the photolysis would not react with the alkene and found that the photolysis of (room temperature) N_2O_5 at 193 nm and 248 nm showed the greatest potential. We tried both wavelengths in the laboratory and observed identical NO_3 spectra (Fig 4.3). We however observed major differences when the excimer was fired with only the reactant, 2-butene, in the flow cell. At 193 nm, we observed formation of large amounts of methyl peroxy radical; at 248 nm, we observed no change in the spectrum. We therefore conducted the photolysis experiments at 248 nm ($\sigma_{248\ nm}(N_2O_5) = 4.19 \times 10^{-19}$ cm^2).[1]

N_2O_5 photolysis however also leads to production of nitrogen dioxide (NO_2). NO_2 can react with both NO_3 and the target species, the 2-NO_3-butyl peroxy radical, to complicate the detection process:[1]

$$NO_2 + NO_3 \rightarrow N_2O_5 \qquad (4.10\ \text{b-d})$$

with $K_{eq(298\ K)} = 2.9 \times 10^{-11}$ cm^3 molec^{-1}

$k_{298\ K}(NO_2 + NO_3 + M) = 7.4 \times 10^{-13}$ cm^3 molec^{-1} s^{-1} at P = 80 Torr

$$CH_3CH(NO_3)CH(OO)CH_3 + NO_2 \leftrightarrow CH_3CH(NO_3)CH(OONO_2)CH_3 \qquad (4.11)$$

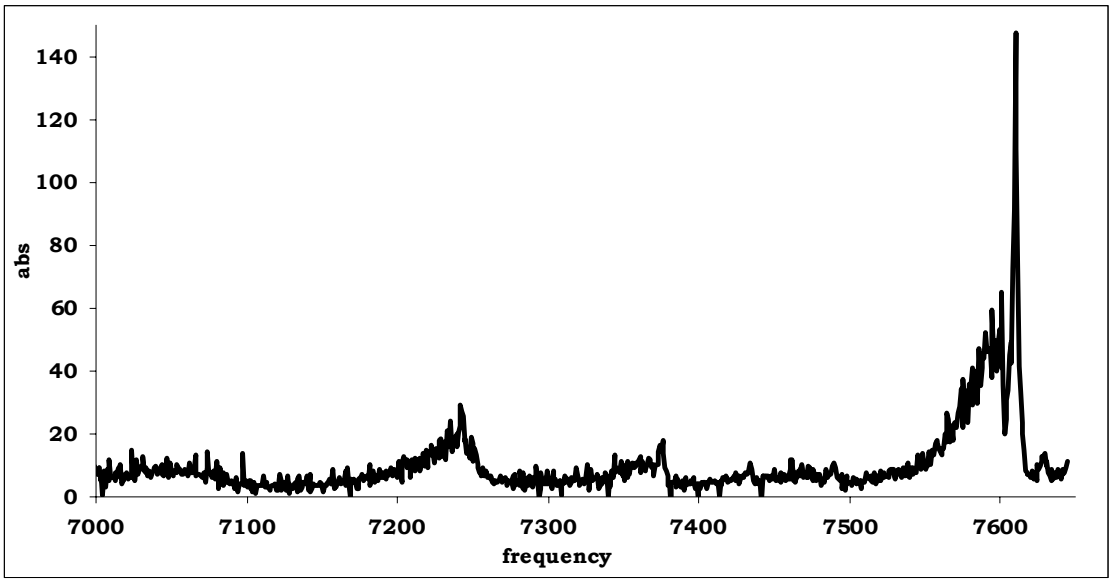

Figure 4.3. CRD spectrum of NO_3 from photolysis of N_2O_5 at 193 nm. Concentrations varied, depending on the vapor pressure of N_2O_5: [NO_3] = 1-10 × 10^{13} molec cm^{-3}. The CRD spectrum of NO_3 from photolysis of N_2O_5 at 248 nm showed slightly lower absorptions; however the scaled features were identical to the spectrum shown here.

To estimate NO_2 yields, we collected time-resolved CRD spectra of the 4_0^1 band of NO_3 at 7602 cm^{-1} and plotted the intensity of the band relative to the time delay of the NIR probe. If we assume that the rate of NO_3 signal decay is from reaction with NO_2 alone, we calculate NO_2 concentrations

~1-10 × 10^{14} molec cm^{-3}. The values are slightly higher than initial NO_3 concentrations, as NO_3 can recombine to form NO_2:[1]

$$NO_3 + NO_3 \rightarrow 2\ NO_2 + O_2 \qquad (4.12\ a\text{-}b)$$

$$k_{298\,K}\ (NO_3 + NO_3) = 2.3 \times 10^{-16}\ cm^3\ molec^{-1}$$

Until we quantitatively characterize the reaction rate between NO_2 and the peroxy radical, we will be unable to do any kinetic experiments using this chemical approach. Direct observation and characterization of the 2-NO_3-butyl peroxy radical however should still be possible and would be a major step in unraveling the complex oxidation scheme.

4.3.2 Apparatus and scan details

The pulsed CRDS apparatus has been described in Chapter 2. We operated the NIR probe and 248-nm excimer lasers at 5 Hz (250 ms residence time) to insure that all gas products were flushed from the cell before excimer fire. To cover the wide NIR wavelength range (7200-8300 cm^{-1}), we used a variety of laser dyes (DCM, Rh 640, Rh 640+610, Rh 610). The optical cavity consisted of a stainless steel photolysis cell with quartz windows, either the 30.5-cm cell with the 17.8-cm × 0.95-cm window or the 24.1-cm cell with the 12.7-cm × 0.95-cm window. 13-cm purge volume couplers were attached at each end of the ringdown cell to protect the CRD mirrors. We used multiple CRD mirrors to cover the NIR range: LGR 1200-nm (R = 99.99%), LGR 1315-nm (R = 99.99%) and Layertec 1390-nm (R = 99.99%) mirrors.

The gas conditions are provided in Fig. 4.4. As the experiment was conducted in smaller segment scans, mass flow meters were placed on each gas inlet for reproducibility. The main valve of the vacuum port was

adjusted to determine the total pressure of the cell. A needle valve was added to the port for additional fine control, as the pump conditions fluctuated during the course of the experiment.

The probe laser was generally delayed 100 μs after excimer fire or chemical initiation. Scans were collected at 0.4 cm^{-1} step size with the excimer on and off for N_2O_5 and N_2O_5/2-butene gas mixtures separately. Preparation of N_2O_5 and 2-butene gas was described in Appendix 3.3 and Appendix 2.4 respectively. Experiments were run at total pressure 80 Torr, with N_2O_5 ~1.5 Torr, 2-butene/N_2 mixture (15%) ~10 Torr, zero grade air ~60 Torr, and N_2 purge ~10 Torr. To confirm that the observed bands were not from 2-butene, we also obtained scans of 2-butene and zero grade air (background) in the 7000-7400 cm^{-1} region. For peroxy verification experiments, we added a nitric oxide (NO, 1% in N_2 from Matheson) port to the ringdown cell.

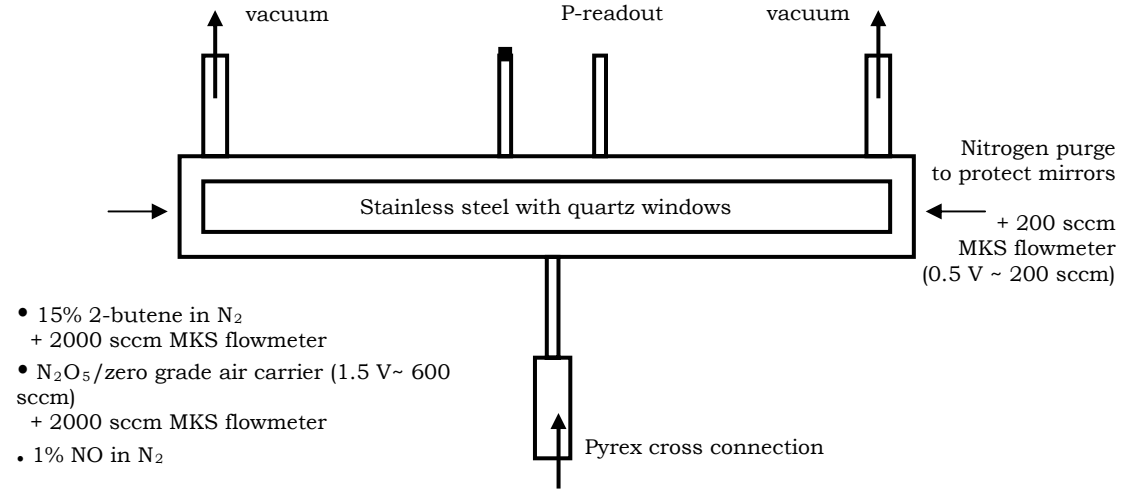

Figure 4.4. Schematic of the photolysis cell for the NO_3 + 2-butene experiment. Details of the gas flow conditions are also provided in the figure. The detection limit of the pulsed CRDS apparatus for the NO_3-peroxy radical is ~ 10^{12} molec cm^{-3}.

4.4 Results and discussion

4.4.1 Observed spectra

CRD spectra of "NO_3 + 2-butene" were obtained from differences between the N_2O_5/2-butene scans with the excimer on and off (Fig. 4.5 a). As NO_3 concentrations determine the final concentrations of 2-NO_3-butyl peroxy radicals, CRD spectra of NO_3 were also collected from differences between N_2O_5 scans with the excimer on and off (Fig. 4.5 b). NO_3 concentrations varied from successive scanning segments. We therefore used NO_3 absorption features to scale overlapping spectra. The same scaling factors were used to overlap the "NO_3 + 2-butene" spectra.

Given the relatively slow reaction rate constant between NO_3 and 2-butene, not all of the NO_3 reactant was consumed during the flow cell experiment. The concentration of 2-butene could not be further increased, as 2-butene has absorptions in the NIR region (Fig. 4.6). While contributions from 2-butene absorption is efficiently removed by subtraction, absorptions from NO_3 have to be manually subtracted from the "NO_3+2-butene" spectra. Analysis of each scanning segment showed that ~60 % of NO_3 was consumed by 2-butene. The corrected spectra were then combined into one spectrum. As the observed absorptions were broad with respect to the step size of the scan (0.4 cm^{-1}), we averaged every five data points for the plot.

The combined CRD spectrum of 2-NO_3-butyl peroxy radical is shown in Fig. 4.5 c. The most intense and broad absorption in the 7250 cm^{-1} - 7800 cm^{-1} region is assigned to the origin band of the $\tilde{A} \leftarrow \tilde{X}$ transition. The small bumps in the absorption belong to different conformers of the 2-NO_3-butyl peroxy radical. We mentioned beforehand that peroxy

radicals have distinct torsional absorptions 500 cm^{-1} and 1000 cm^{-1} to the blue of the origin band. We observe small absorption at 8000 cm^{-1} and 8516 cm^{-1} that are assigned to the COO bend and OO stretch respectively.

The experiments were repeated at low pressure (~40 Torr) and higher 2-butene concentrations (×2). No change in the relative shape or intensities of the bands was observed in the spectra. A weak but sharp absorption was observed at 7383 cm^{-1} and attributed to methyl peroxy radical, CH_3O_2.[55] The absorption was observed as early as 15 μs after the excimer fire, so it cannot be arising from secondary chemistry. Earlier tests on the photolysis of 2-butene at 248 nm did not report any CH_3O_2 production; it maybe that the sensitivity of the CRDS alignment was improved for the NO_3 + 2-butene scans. Some of the NO_3-peroxy radicals may also have enough internal energy to break apart into smaller fragments. Regardless, the CH_3O_2 yield was negligible and did not interfere with the spectral analysis.

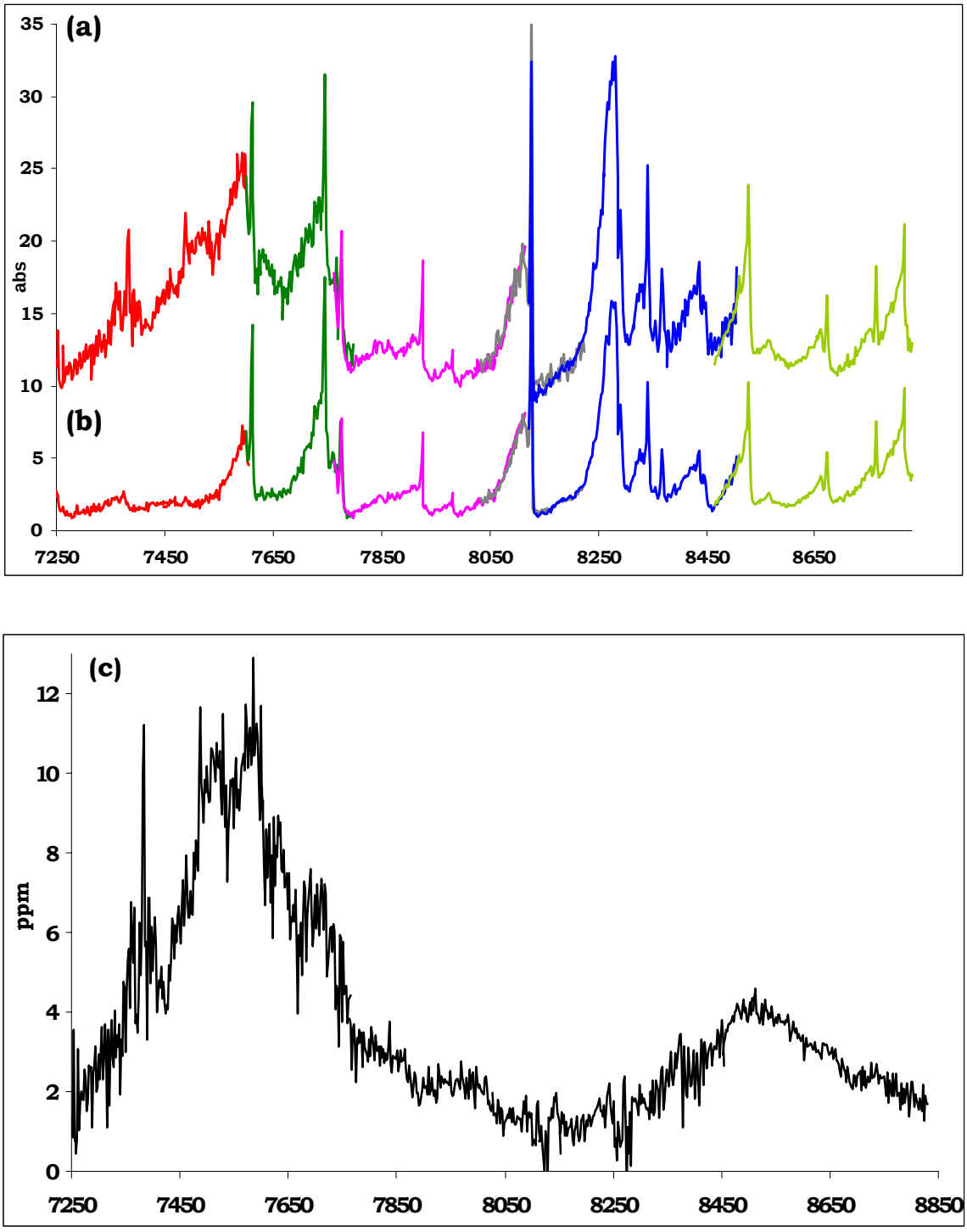

Figure 4.5. CRD spectra of (a) NO_3+2-butene (difference between the N_2O_5/2-butene scans with the excimer on and off) with a 10 ppm offset (b) NO_3 (difference between N_2O_5 scans with the excimer on and off), and (c) 2-NO_3-butyl peroxy radical (spectrum b - spectrum a). The colors indicate the different scanning segments. All spectra shown in the figure have been 5-point averaged.

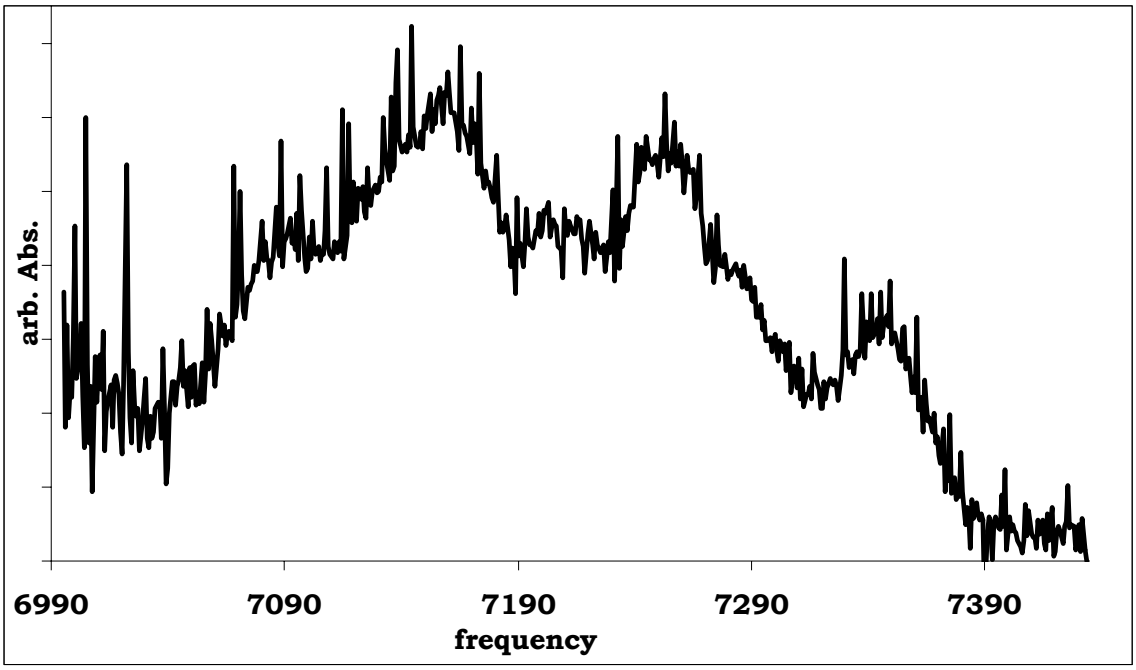

Figure 4.6. CRD spectrum of 2-butene in the 7000 - 7400 cm^{-1} region. The absorption features are flat after 7390 cm^{-1}.

4.4.2 Verification of the peroxy radical spectrum

Observation of the torsional features, in addition to the origin band, is a strong indicator that the spectral absorptions belong to the 2-NO_3-butyl peroxy radical. The shape and absorption frequencies are similar to the spectral features of *sec*-butyl peroxy radical. As NO_3 concentrations determine the amount of peroxy radical generated in the experiment, we can also compare the two concentrations to check whether the values are consistent to first order. While the observation of multiple bumps in the 7250-7600 cm^{-1} region suggest multiple conformers of the 2-NO_3-butyl peroxy radical were formed, they all should have similar absorption cross sections. Thus, we estimate the total concentration of peroxy radical from the observed peak signal at ~10 ppm. The absorption cross section for perxoy radicals in the NIR region has only been measured for ethyl perxoy radical ($CH_3CH_2O_2$), $\sigma_{7596\ cm\text{-}1}(CH_3CH_2O_2) = 5.29 \times 10^{-21}\ cm^2$.[57] We estimate the cross section for 2-NO_3-butyl peroxy radical to be σ_{NIR} ~

10^{-20} ~ 10^{-21} cm^2. Assuming L_R = 17.8-cm (our long photolysis cell), we calculate:

$$[\text{2-NO}_3\text{-butyl peroxy radical}] \sim \frac{10 \times 10^{-6}}{5 \times 10^{-21} \times 17.8} \approx 10^{14} \frac{\text{molec}}{\text{cm}^3} \quad (4.13)$$

This is consistent with the amount of NO_3 generated during photolysis.

Additional experiments were also conducted to verify the spectral assignment. The lifetime for peroxy radicals is typically on the millisecond timescale. The presence of NO_2 will cause the peroxy radical concentration to decrease more quickly (rxn 4.10). We collected time-resolved spectra of the 7250 cm^{-1} - 7650 cm^{-1} region from 100 µs to 10 ms after chemical initiation. As expected, the peroxy radical signal decayed over time and disappeared by >5 ms.

We also injected NO into the system, as NO should react with the peroxy radical rapidly:[1,66]

$$RO_2 + NO \rightarrow RO + NO_2 \quad (4.14)$$

$$k_{298\,K}(RO_2 + NO) \sim 1 \times 10^{-11}\ cm^3\ molec^{-1}$$

The peroxy radical signal disappeared accordingly. All tests therefore indicated that the absorptions observed in the CRD spectrum belonged to the 2-NO_3-butyl peroxy radical.

4.5 Summary

We observed 2-NO_3-butyl peroxy radical in the gas phase for the first time using pulsed CRDS. We were able to observe the radical *in situ* via the $\tilde{A} \leftarrow \tilde{X}$ transition in the NIR region. Although the absorption is much weaker in the NIR than in the UV region, the spectrum has very distinctive structural features. Identification is also easier, as there is less spectral interference from other atmospheric species.

This was the first work to observe NO_3-substituted peroxy radical in any wavelength region or from any alkene oxidation system. Due to the atmospheric importance of NO_3-alkene oxidation, we plan to build on this work by examining larger NO_3-peroxy radicals. We are currently in the process of looking at the NO_3-initiated oxidation of 2-methyl-2-butene and isoprene. 2-methyl-2-butene is structurally similar to 2-butene, with only an extra methyl group on the double bond. As the symmetry is now broken, we should now observe two distinct isomers in the spectra. Studying the NO_3 oxidation of isoprene will be more difficult, as multiple isomers are formed. In the future, we plan to further elucidate the NO_3 oxidation mechanism by coupling the pulsed CRDS apparatus with a chemical ionization mass spectrometer that is equipped to detect multiple products, including the epoxide channel. Thus, we will be able to study the competing pathways of NO_3-initiated oxidation of alkenes simultaneously.

We build on this work in the next chapter, by studying another important subset of substituted peroxy radicals in the atmosphere, Cl-peroxy radicals. We outline preliminary work on both the detection and kinetics of Cl-peroxy radical intermediates to elucidate the mechanism of Cl-initiated oxidation of alkenes.

4.6 References

(1) Sander, S. P.; Friedl, R. R.; Golden, D. M.; Kurylo, M.; Moortgat, G. K.; Wine, P. H.; Ravishankara, A. R.; Kolb, C. E.; Molina, M. J.; Finlayson-Pitts, B. J.; Huie, R. E.; Orkin, V. L. 2006.

(2) Atkinson, R. *Journal of Physical and Chemical Reference Data* **1991**, *20*, 459.

(3) Atkinson, R. *Atmospheric Environment* **2000**, *34*, 2063.

(4) Atkinson, R.; Arey, J. *Chemical Reviews* **2003**, *103*, 4605.

(5) Finlayson-Pitts, B. J.; Pitts, J. N. *Chemistry of the Upper and Lower Atmosphere: Theory, Experiments, and Applications*; Academic Press, 1999.

(6) Ng, N. L.; Kwan, A. J.; Surratt, J. D.; Chan, A. W. H.; Chhabra, P. S.; Sorooshian, A.; Pye, H. O. T.; Crounse, J. D.; Wennberg, P. O.; Flagan, R. C.; Seinfeld, J. H. *Atmospheric Chemistry and Physics* **2008**, *8*, 4117.

(7) Seinfeld, J. H.; Pandis, S. N. *Atmospheric Chemistry and Physics*; Wiley-Interscience, 1997.

(8) Wayne, R. P.; Barnes, I.; Biggs, P.; Burrows, J. P.; Canosamas, C. E.; Hjorth, J.; Lebras, G.; Moortgat, G. K.; Perner, D.; Poulet, G.; Restelli, G.; Sidebottom, H. *Atmospheric Environment Part a-General Topics* **1991**, *25*, 1.

(9) Brown, S. S.; Degouw, J. A.; Warneke, C.; Ryerson, T. B.; Dube, W. P.; Atlas, E.; Weber, R. J.; Peltier, R. E.; Neuman, J. A.; Roberts, J. M.; Swanson, A.; Flocke, F.; McKeen, S. A.; Brioude, J.; Sommariva, R.; Trainer, M.; Fehsenfeld, F. C.; Ravishankara, A. R. *Atmospheric Chemistry and Physics* **2009**, *9*, 3027.

(10) Brown, S. S.; Dube, W. P.; Osthoff, H. D.; Stutz, J.; Ryerson, T. B.; Wollny, A. G.; Brock, C. A.; Warneke, C.; De Gouw, J. A.; Atlas, E.; Neuman, J. A.; Holloway, J. S.; Lerner, B. M.; Williams, E. J.; Kuster, W. C.; Goldan, P. D.; Angevine, W. M.; Trainer, M.; Fehsenfeld, F. C.; Ravishankara, A. R. *Journal of Geophysical Research-Atmospheres* **2007**, *112*.

(11) Brown, S. S.; Neuman, J. A.; Ryerson, T. B.; Trainer, M.; Dube, W. P.; Holloway, J. S.; Warneke, C.; de Gouw, J. A.; Donnelly, S. G.; Atlas, E.; Matthew, B.; Middlebrook, A. M.; Peltier, R.; Weber, R. J.; Stohl, A.; Meagher, J. F.; Fehsenfeld, F. C.; Ravishankara, A. R. *Geophysical Research Letters* **2006**, *33*.

(12) Fry, J. L.; Kiendler-Scharr, A.; Rollins, A. W.; Wooldridge, P. J.; Brown, S. S.; Fuchs, H.; Dube, W.; Mensah, A.; dal Maso, M.; Tillmann, R.; Dorn, H. P.; Brauers, T.; Cohen, R. C. *Atmospheric Chemistry and Physics* **2009**, *9*, 1431.
(13) Spittler, M.; Barnes, I.; Bejan, I.; Brockmann, K. J.; Benter, T.; Wirtz, K. *Atmospheric Environment* **2006**, *40*, S116.
(14) Yang, B.; Meng, J. W.; Zhang, Y.; Liu, C. G.; Gan, J.; Shu, J. N. *Atmospheric Environment* **2011**, *45*, 2074.
(15) Gong, H. M.; Matsunaga, A.; Ziemann, P. J. *Journal of Physical Chemistry A* **2005**, *109*, 4312.
(16) Lim, Y. B.; Ziemann, P. J. *Environmental Science & Technology* **2005**, *39*, 9229.
(17) Bruns, E. A.; Perraud, V.; Zelenyuk, A.; Ezell, M. J.; Johnson, S. N.; Yu, Y.; Imre, D.; Finlayson-Pitts, B. J.; Alexander, M. L. *Environmental Science & Technology* **2010**, *44*, 1056.
(18) Rollins, A. W.; Kiendler-Scharr, A.; Fry, J. L.; Brauers, T.; Brown, S. S.; Dorn, H. P.; Dube, W. P.; Fuchs, H.; Mensah, A.; Mentel, T. F.; Rohrer, F.; Tillmann, R.; Wegener, R.; Wooldridge, P. J.; Cohen, R. C. *Atmospheric Chemistry and Physics* **2009**, *9*, 6685.
(19) Pye, H. O. T.; Chan, A. W. H.; Barkley, M. P.; Seinfeld, J. H. *Atmospheric Chemistry and Physics* **2010**, *10*, 11261.
(20) Fuchs, H.; Dube, W. P.; Cicioira, S. J.; Brown, S. S. *Analytical Chemistry* **2008**, *80*, 6010.
(21) Ingold, K. U. *Accounts of Chemical Research* **1969**, *2*, 1.
(22) Wallington, T. J.; Dagaut, P.; Kurylo, M. J. *Chemical Reviews* **1992**, *92*, 667.
(23) Monks, P. S. *Chemical Society Reviews* **2005**, *34*, 376.
(24) Batt, L. *International Reviews in Physical Chemistry* **1987**, *6*, 53.
(25) Tyndall, G. S.; Cox, R. A.; Granier, C.; Lesclaux, R.; Moortgat, G. K.; Pilling, M. J.; Ravishankara, A. R.; Wallington, T. J. *Journal of Geophysical Research-Atmospheres* **2001**, *106*, 12157.
(26) Lightfoot, P. D.; Cox, R. A.; Crowley, J. N.; Destriau, M.; Hayman, G. D.; Jenkin, M. E.; Moortgat, G. K.; Zabel, F. *Atmospheric Environment Part a - General Topics* **1992**, *26*, 1805.
(27) Benter, T.; Liesner, M.; Schindler, R. N.; Skov, H.; Hjorth, J.; Restelli, G. *Journal of Physical Chemistry* **1994**, *98*, 10492.
(28) Olzmann, M.; Benter, T.; Liesner, M.; Schindler, R. N. *Atmos. Environ.* **1994**, *28*, 2677.
(29) Skov, H.; Benter, T.; Schindler, R. N.; Hjorth, J.; Restelli, G. *Atmos. Environ.* **1994**, *28*, 1583.

(30) Bukhtiyarov, V. I.; Nizovskii, A. I.; Bluhm, H.; Haevecker, M.; Kleimenov, E.; Knop-Gericke, A.; Schloegl, R. *Journal of Catalysis* **2006**, *238*, 260.
(31) Hjorth, J.; Jensen, N. R.; Skov, H.; Capellani, F.; Restelli, G. *Transport and Chemical Transformation of Pollutants in the Troposphere* **1997**, *3*, 113.
(32) Hjorth, J.; Lohse, C.; Nielsen, C. J.; Skov, H.; Restelli, G. *Journal of Physical Chemistry* **1990**, *94*, 7494.
(33) Kholdeeva, O. A.; Khavrutskii, I. V.; Romannikov, V. N.; Tkachev, A. V.; Zamaraev, K. I. *Studies in Surface Science and Catalysis* **1997**, *110*, 947.
(34) Skov, H.; Hjorth, J.; Lohse, C.; Jensen, N. R.; Restelli, G. *Atmospheric Environment, Part A: General Topics* **1992**, *26A*, 2771.
(35) Dlugokencky, E. J.; Howard, C. J. *Journal of Physical Chemistry* **1989**, *93*, 1091.
(36) Berndt, T. *Preprints - American Chemical Society, Division of Petroleum Chemistry* **2007**, *52*, 271.
(37) Berndt, T.; Boege, O. *Berichte der Bunsen-Gesellschaft* **1994**, *98*, 869.
(38) Berndt, T.; Boege, O. *Journal of Atmospheric Chemistry* **1995**, *21*, 275.
(39) Berndt, T.; Boege, O.; Rolle, W. *Environmental Science and Technology* **1997**, *31*, 1157.
(40) Berndt, T.; Boge, O. *International Journal of Chemical Kinetics* **1997**, *29*, 755.
(41) Berndt, T.; Boge, O. *Journal of the Chemical Society, Faraday Transactions* **1997**, *93*, 3021.
(42) Zhao, J.; Zhang, R. *Atmos. Environ.* **2008**, *42*, 5849.
(43) Cole-Filipiak, N. C.; O'Connor, A. E.; Elrod, M. J. *Environmental Science & Technology* **2010**, *44*, 6718.
(44) Minerath, E. C.; Elrod, M. J. *Environmental Science & Technology* **2009**, *43*, 1386.
(45) Herrick, R. F.; Smith, T. J.; Ellenbecker, M. J. *American Industrial Hygiene Association Journal* **1987**, *48*, 773.
(46) Paulot, F.; Crounse, J. D.; Kjaergaard, H. G.; Kurten, A.; St Clair, J. M.; Seinfeld, J. H.; Wennberg, P. O. *Science* **2009**, *325*, 730.
(47) IPCC *Climate Change 2007: Synthesis Report. Contribution of Working Groups I, II, and III to the Fourth Assessment, Report of the Intergovernmental Panel on Climate Change, Geneva, Switzerland*, 2007.
(48) Perez-Casany, M. P.; Nebot-Gil, I.; Sanchez-Marin, J.; Tomas-Vert, F.; Martinez-Ataz, E.; Cabanas-Galan, B.;

Aranda-Rubio, A. *Journal of Organic Chemistry* **1998**, *63*, 6978.
(49) Perez-Casany, M. P.; Nebot-Gil, I.; Sanchez-Marin, J. *J. Phys. Chem. A* **2000**, *104*, 10721.
(50) Cartas-Rosado, R.; Raul Alvarez-Idaboy, J.; Galano-Jimenez, A.; Vivier-Bunge, A. *Theochem* **2004**, *684*, 51.
(51) Cartas-Rosado, R.; Santoyo, M. E. R.; Alvarez-Idaboy, J. R.; Vivier-Bunge, A. *J. Phys. Chem. A* **2001**, *105*, 9222.
(52) Nguyen, T. L.; Park, J.; Lee, K.; Song, K.; Barker, J. R. *The Journal of Physical Chemistry A* **2011**, null.
(53) Chung, C.-Y.; Cheng, C.-W.; Lee, Y.-P.; Liao, H.-Y.; Sharp, E. N.; Rupper, P.; Miller, T. A. *Journal of Chemical Physics* **2007**, *127*, 044311/1.
(54) Glover, B. G.; Miller, T. A. *J. Phys. Chem. A* **2005**, *109*, 11191.
(55) Just, G. M. P.; McCoy, A. B.; Miller, T. A. *Journal of Chemical Physics* **2007**, *127*, 044310/1.
(56) Just, G. M. P.; Sharp, E. N.; Zalyubovsky, S.; Miller, T. A. *Abstracts of Papers, 231st ACS National Meeting, Atlanta, GA, United States, March 26-30, 2006* **2006**, PHYS.
(57) Melnik, D.; Chhantyal-Pun, R.; Miller, T. A. *Journal of Physical Chemistry A* **2010**, *114*, 11583.
(58) Pushkarsky, M. B.; Zalyubovsky, S. J.; Miller, T. A. *Journal of Chemical Physics* **2000**, *112*, 10695.
(59) Rupper, P.; Sharp, E. N.; Tarczay, G.; Miller, T. A. *J. Phys. Chem. A* **2007**, *111*, 832.
(60) Sharp, E., N.; Rupper, P.; Miller, T., A. *The journal of physical chemistry. A* **2008**, *112*, 1445.
(61) Sharp, E. N.; Rupper, P.; Miller, T. A. *Physical Chemistry Chemical Physics* **2008**, *10*, 3955.
(62) Chhantyal-Pun, R.; Kline, N. D.; Thomas, P. S.; Miller, T. A. *Journal of Physical Chemistry Letters* **2010**, *1*, 1846.
(63) Zalyubovsky, S. J.; Wang, D.; Miller, T. A. *Chemical Physics Letters* **2001**, *335*, 298.
(64) Deev, A., *Ph. D. Thesis*, California Institute of Technology, 2005.
(65) M. J. Frisch, G. W. T., H. B. Schlegel, G. E. Scuseria, M. A. Robb, J. R. Cheeseman, V. G. Zakrzewski, J. A. Montgomery, Jr., R. E. Stratmann, J. C. Burant, S. Dapprich, J. M. Millam, A. D. Daniels, K. N. Kudin, M. C. Strain, O. Farkas, J. Tomasi, V. Barone, M. Cossi, R. Cammi, B. Mennucci, C. Pomelli, C. Adamo, S. Clifford, J. Ochterski, G. A. Petersson, P. Y. Ayala, Q. Cui, K. Morokuma, D. K. Malick, A. D. Rabuck, K. Raghavachari, J. B. Foresman, J. Cioslowski, J. V. Ortiz, B. B. Stefanov, G. Liu, A. Liashenko, P. Piskorz, I.

Komaromi, R. Gomperts, R. L. Martin, D. J. Fox, T. Keith, M. A. Al-Laham, C. Y. Peng, A. Nanayakkara, C. Gonzalez, M. Challacombe, P. M. W. Gill, B. Johnson, W. Chen, M. W. Wong, J. L. Andres, C. Gonzalez, M. Head-Gordon, E. S. Replogle, and J. A. Pople, *Gaussian 98*, Gaussian, Inc.: Pittsburgh, PA, 1998.

(66) Atkinson, R.; Baulch, D. L.; Cox, R. A.; Crowley, J. N.; Hampson, R. F.; Hynes, R. G.; Jenkin, M. E.; Rossi, M. J.; Troe, J. *Atmos. Chem. Phys.* **2006**, *6*, 3625.